Zuo *et al. Cell Communication and Signaling* (2024) 22:236
https://doi.org/10.1186/s12964-024-01604-y

Cell Communication and Signaling

RESEARCH Open Access

Interleukin-4 protects retinal ganglion cells and promotes axon regeneration

Zhaoyang Zuo[1†], Bin Fan[1†], Ziyuan Zhang[1], Yang Liang[1], Jing Chi[1] and Guangyu Li[1*]

Abstract

Background The preservation of retinal ganglion cells (RGCs) and the facilitation of axon regeneration are crucial considerations in the management of various vision-threatening disorders. Therefore, we investigate the efficacy of interleukin-4 (IL-4), a potential therapeutic agent, in promoting neuroprotection and axon regeneration of retinal ganglion cells (RGCs) as identified through whole transcriptome sequencing in an in vitro axon growth model.

Methods A low concentration of staurosporine (STS) was employed to induce in vitro axon growth. Whole transcriptome sequencing was utilized to identify key target factors involved in the molecular mechanism underlying axon growth. The efficacy of recombinant IL-4 protein on promoting RGC axon growth was validated through in vitro experiments. The protective effect of recombinant IL-4 protein on somas of RGCs was assessed using RBPMS-specific immunofluorescent staining in mouse models with optic nerve crush (ONC) and N-methyl-D-aspartic acid (NMDA) injury. The protective effect on RGC axons was evaluated by anterograde labeling of cholera toxin subunit B (CTB), while the promotion of RGC axon regeneration was assessed through both anterograde labeling of CTB and immunofluorescent staining for growth associated protein-43 (GAP43).

Results Whole-transcriptome sequencing of staurosporine-treated 661 W cells revealed a significant upregulation in intracellular IL-4 transcription levels during the process of axon regeneration. In vitro experiments demonstrated that recombinant IL-4 protein effectively stimulated axon outgrowth. Subsequent immunostaining with RBPMS revealed a significantly higher survival rate of RGCs in the rIL-4 group compared to the vehicle group in both NMDA and ONC injury models. Axonal tracing with CTB confirmed that recombinant IL-4 protein preserved long-distance projection of RGC axons, and there was a notably higher number of surviving axons in the rIL-4 group compared to the vehicle group following NMDA-induced injury. Moreover, intravitreal delivery of recombinant IL-4 protein substantially facilitated RGC axon regeneration after ONC injury.

Conclusion The recombinant IL-4 protein exhibits the potential to enhance the survival rate of RGCs, protect RGC axons against NMDA-induced injury, and facilitate axon regeneration following ONC. This study provides an experimental foundation for further investigation and development of therapeutic agents aimed at protecting the optic nerve and promoting axon regeneration.

†Dr. Zhaoyang Zuo and Dr. Bin Fan contribute equally to this paper and should be regarded as co-first authors.

*Correspondence:
Guangyu Li
liguangyu@aliyun.com

Full list of author information is available at the end of the article

Keywords Retinal ganglion cells, Optic nerve crush, Nerve excitotoxicity, Axon regeneration

Background

Retinal ganglion cell (RGC) death and axon loss constitute the primary pathological characteristics of various blinding disorders, including glaucoma and traumatic optic neuropathy. Consequently, protecting RGCs and facilitating the regeneration of RGC axons emerge as pivotal concerns in the therapeutic management of these diseases.

Staurosporine (STS) is a broad-spectrum inhibitor of protein kinase C (PKC). It has been demonstrated that high concentrations of staurosporine can induce apoptosis in nerve cells [1]. Conversely, at nanomolar levels, staurosporine significantly protects retinal ganglion cells in mice with optic nerve injury [2]. In vitro studies have revealed that low concentrations of staurosporine effectively promote the growth and development of neurons or neuron-like cells such as HN33 and PC12, promoting the formation of axon-like structures [3, 4]. Furthermore, Kim et al. reported that treatment with 50 nM staurosporine for 12 h induces differentiation in chicken embryonic retinal ganglion cells [5]. These findings collectively suggest that low concentrations of staurosporine activate a shared molecular mechanism to enhance axon outgrowth across various neuronal types. This knowledge may serve as a foundation for identifying crucial targets involved in retinal ganglion cell protection and axon regeneration in vitro.

Furthermore, extracellular factors, especially cytokines, also play a crucial role in the process of axon regeneration. Cytokines are multifunctional and multi-effect proteins that not only participate in immune responses but also participate in pathological processes after central nervous system (CNS) injury. Numerous studies have demonstrated that local T cells are stimulated, activated and secrete different cytokines after neuron injury in CNS of mice and rats [6]. Additionally, Fischer et al. revealed that continuous expression of hyper-IL-6 directly targeting the gp130 receptor can activate JAK/STAT3 and PI3K/AKT/mTOR signaling pathways with greater effect on promoting axon regeneration of retinal ganglion cells than other known treatments (such as *PTEN* knockout) [7]. Bethea et al. reported that IL-10 inhibited TNF-α production and promoted axon regeneration of dorsal root ganglion cells after spinal cord injury in rats [8]. Moreover, Lindborg et al. showed that inhibition of IL-22 could increase the levels of transcription factors and cytokines that play an important role in optic nerve regeneration signals, and significantly promote the axon regeneration of retinal ganglion cells in mice [9]. Consequently, cytokines assume a critical role in neuroprotection and axon regeneration.

N-methyl-D-aspartic acid receptor (NMDAR) is a subtype of glutamate receptor. Overactivation of NMDARs can trigger calcium influx and excessive production of nitric oxide, leading to apoptosis and subsequent retinal ganglion cell death. N-methyl-D-aspartic acid (NMDA) primarily induces RGC death by nerve excitotoxic damage, followed by anterograde degeneration of RGC axons [10]. However, the optic nerve crush (ONC) model damages the axon structure of the optic nerve through mechanical force, resulting in increased calcium influx, inflammatory response, oxidative stress damage, and ultimately retrograde RGC death [11]. Due to distinct injuries, the processes and molecular mechanisms underlying RGC death and axon degeneration exhibit partially different. In addition, previous studies have shown that different types of RGCs display varying susceptibilities to ONC or NMDA-induced injury. BD-RGC represents the most vulnerable RGC subtype to ONC injury, whereas W3-RGC exhibits heightened sensitivity to the NMDA damage [12]. Utilizing both injury models will facilitate the identification of shared molecular mechanisms and potential therapeutic targets for RGC death caused by diverse injuries.

The present study established an in vitro model of axon growth using staurosporine (50 nM) in 661 W cells. Subsequently, scRNA-seq was employed to screen for the candidate factor IL-4, which plays a crucial role in promoting axon growth. Furthermore, we investigated the protective effect of recombinant IL-4 protein (rIL-4) on retinal ganglion cells (RGCs), as well as its potential to enhance axon regeneration through NMDA and ONC injury models in vivo. These findings lay a solid experimental foundation for the development of novel therapeutic strategies targeting optic nerve protection and regeneration.

Materials and methods

Animals

Five- to six-week-old male C57BL/6J mice (WT) weighing 20 to 25 g were purchased from the Animal Research Center of Jilin University (Changchun, Jilin, China). All mice purchased were housed in a central animal care facility with room temperature maintained at 21 ℃ −23 ℃ and a 12-h light/dark cycle maintained, and mice had free access to food and water. All animal experiments were reviewed and approved by the Ethics Committee of Jilin University and complied with the ARVO Declaration on Animal Research.

Cell culture

661 W cells were gifted to Dr. Muayyad Al-Ubaidi (University of Oklahoma Health Sciences Center, USA). 661 W cells were cultured at 37 °C in a 5% CO_2 cell incubator in Dulbecco's modified Eagle medium (HyClone, Beijing, China) supplemented with 10% fetal bovine serum and 1% penicillin/streptomycin. The cells were passaged every 2–3 days using trypsin-EDTA.

Cell differentiation with STS and rIL-4

The culture was continued for 24 h after the addition of STS to a final concentration of 50 nM or recombinant murine IL-4 protein to a final concentration of 1 μg/mL in each well of a tissue culture six-well plate inoculated with 661 W cells.

Immunofluorescence staining of 661 W cells

The cells were fixed in 4% paraformaldehyde, permeabilized with 0.5% Triton X-100 for 20 min, blocked with 5% BSA for 1 h, and then incubated with the corresponding primary antibody (mouse anti-βIII-Tubulin, 1:100; rabbit anti-NeuN, 1:400, 4 ℃ overnight). The cells were washed three times with PBS (5 min) and incubated with the corresponding secondary antibodies (DyLight 488, anti-mouse IgG, 1:400; Cy3, anti-rabbit IgG, 1:400, 2 h at room temperature in the dark). After further staining of nuclei with DAPI, samples were placed under a fluorescence microscope (Olympus, Japan), observed and photographed. Neurons with positive immunofluorescence staining were traced and analyzed using the SNT plug-in of ImageJ.

Immunoblotting

Cells or retinal tissue were ultrasonically disrupted in 1% protease inhibitor (PMSF) and RIPA protein lysis buffer (Beyotime, Shanghai, China). The protein concentration was measured using a BCA kit (Beyotime, Shanghai, China). Cell lysates were dissolved in an equal volume (20 μg) of sample buffer and boiled at 100 ℃ for 5 min, followed by electrophoresis on an 8–12% SDS-polyacrylamide gel. Next, the proteins were transferred to PVDF membranes. PVDF membranes were blocked with 5% skim milk. The corresponding primary antibodies were then added for incubation (4 ℃, overnight) (anti-NeuN antibody, 1:2000, anti-βIII-tubulin antibody, 1:2000, Beyotime, Shanghai, China). After washing three times (5 min), the corresponding horseradish peroxidase conjugated secondary antibody (anti-rabbit IgG, HRP conjugated/anti-mouse IgG, HRP conjugated, 1:8000, Signalway, Pearland, TX, USA) was added and incubated for 1 h. The target protein blots were visualized using the enhanced chemiluminescence method and photographed with a charge coupled device (CCD) camera (Tanon, Shanghai, China), and the gray value of the protein bands was analyzed by ImageJ software.

mRNA sequencing

The sequencing samples were 50 nM STS-treated 661 W cells and untreated 661 W cell samples in triplicate for each group. Total RNA in cells was isolated using TRIzol (Invitrogen, Carlsbad, CA, USA). The quality was then quantified and assessed using a NanoDrop and Agilent 2100 bioanalyzer (Thermo Fisher Scientific, MA, USA). After mRNA purification using oligonucleotide (dT)-attached magnetic beads, cDNA fragments were generated by reverse transcription with random hexamer primers and amplified by polymerase chain reaction (PCR). After the reaction was purified with Ampure XP Beads, it was dissolved in ethidium bromide solution. Double-stranded PCR products were validated using an Agilent Technologies 2100 bioanalyzer and then heated, denatured, and cycled through splinted oligonucleotide sequences to obtain the final library. The final library was amplified with phi29 to form DNA nanospheres (DNBS) containing more than 300 copies of a single molecule. DNB was loaded into the regular nanoarray, and 50-bp single-end sequencing reads were generated on the BGIseq500 platform (BGI-Shenzhen, China). Clean reads were obtained and stored in FASTQ format after removing reads with adaptor sequences, low-quality base ratios greater than 20% (base quality less than or equal to 5) or unknown bases ("N" base) ratio greater than 5% using SOAPnuke (v1.5.2). The clean reads were mapped to the reference genome using HISAT2 (version: LU_Bosgru_v3.0). The clean reads were aligned to the reference coding gene set using Bowtie2 (v2.2.5), and then the expression of the gene was calculated using RSEM (v1.2.12). Finally, using the R package DESeq2b (v1.4.5) differential expression analysis, data were reported for log2 (STS_samples/Vehicle_samples). The threshold was a$|\log2FoldChange| \geq 1$ or $q \leq 0.05$.

NMDA model, optic nerve crush model and drug administration

After anesthesia with 1% pentobarbital sodium, the pupil of the mouse was dilated with a mixture of 0.5% tropicamide and 0.5% phenylephrine hydrochloride eye drops (Santen, Suzhou, China). Scleral puncturing was performed under an operating microscope using a 32G needle at approximately 1–1.5 mm posterior to the limbus, tilted downward. A 10 μl Hamilton syringe (Hamilton Company, Reno, NV) was attached to a 33 G needle and inserted into the vitreous cavity through the scleral tunnel while avoiding damaging the lens. A total of 1.5 μl of drug was injected into the vitreous cavity each time.

To establish the ONC injury model, adult mice were anesthetized with 1% pentobarbital sodium and placed

under the operating microscope. Oxybuprocaine hydrochloride ophthalmic solution (0.5%; Santen, Suzhou, China) was used for topical anesthesia. Following the blunt separation of the conjunctival sac using two toothed forceps around the lateral canthus, the optic nerve of the left eye was carefully exposed intraorbitally and crushed with self-closing Dumont forceps #5 (Beijing, China) 1 mm behind the globe for 15 s without damaging the ophthalmic artery. Then, rIL-4 (0.1 μg/μl) was injected into the left eye, and vehicle was injected into the fellow eye as a control on days 0 and 3 for the 7-day group. The mice in the 14-day group were treated on days 0, 3, and 7.

To establish the NMDA injury model, NMDA (20 mM) and rIL-4 (0.1 μg/μl) were injected into the left eye, and NMDA and vehicle were injected into the fellow eye on day 0. Then, rIL-4 was injected into the left eye and vehicle was injected into the fellow eye on day 3 for the 7-day group, and on days 3 and 7 for the 14-day group. Cholera toxin B subunit (CTB) was injected into the eyes of the mice 3 days before euthanasia.

Histology

After the mice were anesthetized with 1% sodium pentobarbital, the whole body was perfused with normal saline and 4% PFA for prefixation. Next, the eyeball, optic nerve, optic chiasm, and brain were dissected and isolated. Tissues were fixed in 4% PFA for 24 h followed by dehydration in 30% sucrose for 24 h.

Retinas were isolated from mouse eyeballs, and retinal flat mounts were made. The flat mounts were permeabilized in 0.5% Triton X-100 for 30 min at room temperature and blocked in 10% normal goat serum, 1% BSA and 0.1% Triton X-100 in PBS for 1 h. Next, the flat mounts were incubated overnight in the corresponding primary antibodies (rabbit anti-RBPMS, 1:200). After washing three times (10 min) with PBS, the flat mounts were incubated with the corresponding secondary antibody (DyLight 488, anti-rabbit IgG, 1:400) for 2 h (room temperature) and washed three times (10 min) with PBS. The flat mounts were mounted before being observed under a microscope and photographed. Images of the whole retinal flat mount were stitched from several low-magnification images using Adobe Photoshop software. Twelve images (0.35×0.45 mm^2 each) were taken for each retina at high magnification using a fluorescence microscope (Olympus, Japan). The number of RGCs in each image was counted with the StarDist 2D plug-in in ImageJ software.

To prepare frozen sections of retinas and optic nerves, fixed eyeballs, with anterior segments and vitreous removed, or optic nerves were sectioned (10 μm for axial sections of retinas and optic nerves and 4 μm for cross-sectional sections of optic nerves). For CTB-labeled samples, frozen sections were mounted and observed under a fluorescence microscope (Olympus, Japan).

Frozen sections that needed immunofluorescence staining were washed with PBS and blocked with 10% normal goat serum, 1% BSA, and 0.1% Triton X-100 in PBS for 1 h. Next, the frozen sections were incubated (4 ℃, overnight) with the corresponding primary antibodies (rabbit anti-GAP43, 1:200; mouse anti-β-III Tubulin, 1:100). The sections were washed (10 min) three times with PBS and incubated with the corresponding secondary antibody for 2 h (Cy3, anti-rabbit IgG, 1:400; DyLight 488, anti-mouse IgG, 1:400, room temperature). The slides were washed three times (5 min) with PBS at room temperature, mounted and observed under a fluorescence microscope (Olympus, Japan). For each group of ONC models, the regeneration of axons at a prespecified distance from the injury site was calculated by counting the number of fluorescent positive axons at 500 μm from the injury site and measuring the width of the optic nerve at that location (r is the radius of the optic nerve, t is the section thickness). The total number of regenerated axons with lengths greater than or equal to 500 μm was calculated. The formula is $\Sigma_{ad}=\pi r^2\times$ (average number of axons/width (mm))/t.

After immunofluorescence staining of cross-sectional sections of the optic nerve for β-III tubulin, the number of β-III tubulin-positive axons 1 cm from the injury site was counted using the Stardist plugin in ImageJ. Five 20 μm× 20 μm square areas were taken from each cross-sectional section of optic nerve for analysis, counting, and calculation of density. Then, the mean value of nerve density was calculated for each group.

For CTB labeling in the lateral geniculate body and superior colliculus, mouse brains were collected 3 days after intravitreal injection of CTB. Frozen Sect. (15 μm for LGN and SC) were obtained coronally at the LGN and SC. Thereafter, the frozen sections were mounted with mounting medium. The frozen sections were placed under a fluorescence microscope (Olympus, Japan) for observation and photography.

Flash electroretinogram (ERG)

Flash ERG was performed with the RetiMINER IV system (IRC Medical Equipment, Chongqing, China). For the NMDA injury model, the mice in each group were adapted in darkness overnight before the beginning of experiment. All procedures were performed under a dim red light to maintain scoptic vision. After anesthetizing with tribromoethanol (350 mg/kg), atropine sulfate eye gel was used to dilate pupils. Subsequently, thread electrodes were placed across the center of bilateral cornea. A subcutaneous electrode was inserted subcutaneously between bilateral eyes. A ground electrode was placed at the end of the mouse's tail with conductive

paste. Bilateral ERG recording was performed from both eyes simultaneously, with each item repeated at least twice. The reliability of the recorded waveforms was confirmed by the coincidence among waveforms. Scotopic ERGs were recorded at stimulus intensities levels of 0.001, 0.01, 0.1, 1.0, 3.0, and 10.0 cd·s/m^2. Oscillatory potentials (OPs) were recorded using the white flashes of 3.0 cd·s/m^2 scotopic responses via bandpass filtering between 50 and 170 Hz. The positive scotopic threshold responses (pSTRs) were measured from the baseline to the positive peak of the waveform at a flash intensity of 0.001 cd·s/m^2. After light adaptation for 15 min, the photopic negative responses (PhNRs) were measured from the baseline to the trough of the negative response following the positive b-wave at a flash intensity of 10.0 cd·s/m^2.

Table 1 Chemicals and reagents used in the study

Chemicals	Source	Identifier	Dosage
Staurosporine	Abmole (Beijing, China)	Cat# M2066	
N-methyl-D-aspartic Acid (NMDA)	Abmole	Cat# M2884	
4′,6-diamidino-2-phenylindole (DAPI)	Solarbio (Beijing, China)	Cat# C0065	
Antifading mounting medium	Solarbio	Cat# S2100	
Cholera Toxin Subunit B (CTB) conjugated Alexa Fluor 488	Thermo Fisher Scientific (MA, USA)	Cat# C34775	
recombinant murine IL-4 protein	PeproTech (Rocky Hill, NJ, USA)	Cat# 214 – 14	
Reagents for cell histology	**Source**	**Identifier**	**Dosage**
mouse anti-βIII-Tubulin	Beyotime (Shanghai, China)	Cat# AT809	1:100
rabbit anti-NeuN	Abcam (Cambridge, UK)	Cat# ab177487	1:400
DyLight 488, anti-mouse IgG	Abbkine (Shanghai, China)	Cat# A23210	1:400
Cy3, anti-rabbit IgG	Abbkine	Cat# A22220	1:400
Reagents for Western blot	**Source**	**Identifier**	**Dosage**
mouse anti-β-III Tubulin	Beyotime	Cat# AT809	1:2000
rabbit anti-NeuN	Abcam	Cat# ab177487	1:5000
mouse anti-β-actin	Signalway (Pearland, TX, USA)	Cat# 21,800	1:8000
anti-rabbit IgG, HRP conjugated	Signalway	Cat# L3012	1:8000
anti-mouse IgG, HRP conjugated	Signalway	Cat# L3032	1:8000
Reagents for tissue histology	**Source**	**Identifier**	**Dosage**
rabbit anti-RBPMS	OmnimAbs (California, USA)	Cat# OM165217	1:200
rabbit anti-GAP43	Beyotime	Cat# AF0153	1:200
mouse anti-β-III Tubulin	Beyotime	Cat# AT809	1:100
rabbit anti-IL4R	Affinity Biosciences	Cat# DF8567	1:200
DyLight 488, anti-rabbit IgG	Abbkine	Cat# A23220	1:400
DyLight 488, anti-mouse IgG	Abbkine	Cat# A23210	1:400
Cy3, anti-rabbit IgG	Abbkine	Cat# A22220	1:400

Chemicals and reagents

The chemicals and reagents used in this study are listed in Table 1.

Statistical analysis

All experiments were repeated at least three times, and values are presented as the mean ± standard error of the mean (mean ± SEM). An unpaired two-tailed Student's *t* test was used for comparisons between the two groups. One-way analysis of variance (ANOVA) was used to assess mean differences among multiple groups, followed by Bonferroni post hoc correction or Dunn's nonparametric Kruskal–Wallis test for multiple comparisons. ImageJ software was used to measure the gray value of the Western blot results. GraphPad Prism version 9.0.0 for Windows (GraphPad Software, San Diego, CA, USA) was used for data processing, analysis, and plotting. A value of $p < 0.05$ was considered statistically significant.

Results

STS induces differentiation and axon outgrowth of 661 W cells

As depicted in Fig. 1A, treatment of 661 W cells with a concentration of 50 nM STS for a duration of 6 h significantly facilitated the growth of axon-like structures. Immunofluorescence staining further confirmed the strong positivity of β-III tubulin in these developing neurites (Fig. 1B). Additionally, compared to the vehicle group, the STS-treated group exhibited a substantial increase in neurite extension length (Fig. 1C). Furthermore, immunostaining and Western blot results demonstrated significant upregulation of neuronal markers such as NeuN and β-III tubulin in STS-treated 661 W cells, indicating that STS effectively induced differentiation into mature neurons (Fig. 1D-F).

To elucidate the molecular mechanism underlying STS-induced axon outgrowth, we conducted whole transcriptome RNA sequencing on 661 W cells treated with STS. Based on the differential expression of genes in response to STS treatment, upregulated and downregulated genes were ranked according to their transcriptional changes. Notably, the transcription level of IL-4 was significantly increased (Fig. 2A). Subsequently, we employed the Gene Ontology (GO) database for enrichment and analysis of biological processes, cellular components, molecular functions. We also KEGG pathway

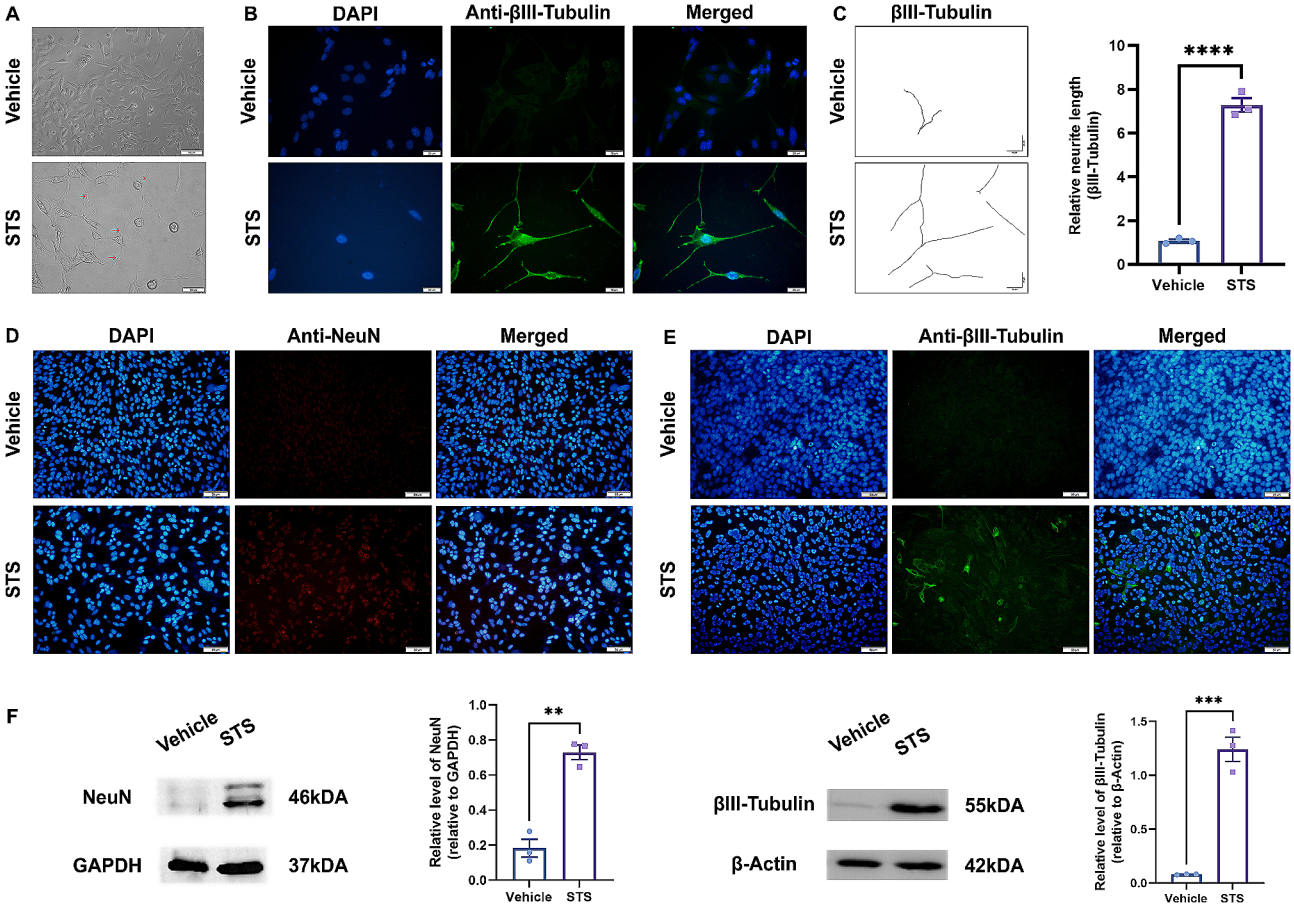

Fig. 1 Induction of axon outgrowth in 661 W cells by STS. **A**: Light microscopy showed that 661 W cells treated with 50 nM STS for 6 h extended long axon-like structures (indicated by red arrows). **B**: The extended axon-like structures of 661 W cells treated with 50 nM STS showed positive immunofluorescence staining for βIII-tubulin. C: Neurite tracing showed that the extended neurites of 661 W cells treated with 50 nM STS were longer than those treated with vehicle. D, E: Higher fluorescence intensity of NeuN (red) and βIII-tubulin (green) was observed in 661 W cells treated with STS. F: Western blot results showed that the protein levels of NeuN and βIII-tubulin were higher in 661 W cells treated with STS. n = 3 per group, ** indicates $p < 0.01$, *** indicates $p < 0.005$, **** indicates $p < 0.001$

analysis with upregulated genes following STS treatment. Our KEGG pathway analysis revealed that differentially transcribed genes primarily participated in inflammation-related signaling pathways including the IL-17 signaling pathway, MAPK pathway, and autophagy pathway (Fig. 2B and C). Furthermore, protein-protein interaction analysis demonstrated that IL-4 occupied a central position within the network of upregulated signals in 661 W cells (Fig. 2D). Collectively, these findings suggest that IL-4 may represent a promising molecular target through which STS promotes axon growth.

Recombinant IL-4 protein promotes the differentiation and axon outgrowth of 661 W cells

Subsequently, we investigated the favorable impact of recombinant IL-4 protein on axon growth in 661 W cells. Following a 24-hour treatment with 1 μg/mL recombinant IL-4 protein, noticeable growth of axon-like structures was observed in the treated 661 W cells (Fig. 3A). These developing structures exhibited positive staining for βIII-tubulin (Fig. 3B) and displayed longer extensions compared to those in the vehicle group (Fig. 3C). Furthermore, treatment with recombinant IL-4 protein induced specific neuronal characteristics in the 661 W cells, as evidenced by significantly increased expression levels of NeuN and βIII-tubulin (Fig. 3D, E). Western blot analysis also confirmed a significant upregulation of NeuN and βIII-tubulin expression in the recombinant IL-4-treated 661 W cells (Fig. 3F). In conclusion, our findings demonstrate that recombinant IL-4 protein effectively promotes axon growth in 661 W cells similar to the effects exerted by STS.

Recombinant IL-4 protein protected RGSs from NMDA damage

To further investigate the effects of the recombinant IL-4 protein on RGCs, two animal models of RGC axon injury were established. Initially, we examined the expression

A

UP-REGULATED	Gene ID	Gene Symbol	log2 (STS_661W / Control_661W)	DOWN-REGULATED	Gene ID	Gene Symbol	log2 (STS_661W / Control_661W)
1	12919	Crhbp	6.243313926	1	11548	Adra1b	-5.456104408
2	140919	Slc17a6	6.124828999	2	72077	Gcnt3	-5.322044218
3	20608	Sstr4	6.049537439	3	209387	Trim30d	-5.265507313
4	630994	Lce3d	6.027171572	4	108169098	Gm46934	-5.248361862
5	18716	Pip	5.716552739	5	231655	Oasl1	-5.113898023
6	16189	Il4	5.489823864	6	15957	Ifit1	-5.020234826
7	100041230	Hist1h4m	5.142624197	7	24131	Ldb3	-4.830574346
8	20310	Cxcl2	4.903974488	8	71026	Speer3	-4.652333281
9	15370	Nr4a1	4.887825215	9	105833	Ccdc65	-4.555819986
10	241431	Xirp2	4.78829906	10	332923	Gm12794	-4.466539156
11	15160	Serpind1	4.637874243	11	30927	Snai3	-4.463695043
12	67310	Pdlim3	4.602155401	12	234796	Klhl36	-4.435118127
13	239845	Gpr156	4.560621385	13	667370	Ifit3b	-4.402155667
14	14825	Cxcl1	4.487693587	14	26434	Pmp	-4.391500324
15	15896	Icam2	4.377662768	15	30878	Apln	-4.315019342
16	18168	Npy5r	4.362789826	16	15945	Cxcl10	-4.04843874
17	110187	Scgb2b26	4.297095916	17	16145	Igtp	-4.034327431
18	71740	Nectin4	4.277244674	18	241568	Lrrc4c	-3.951172589
19	76974	Urah	4.209999162	19	75761	Apol7a	-3.847383555
20	20770	Muc2	4.204079187	20	223672	Apol9a	-3.733870028

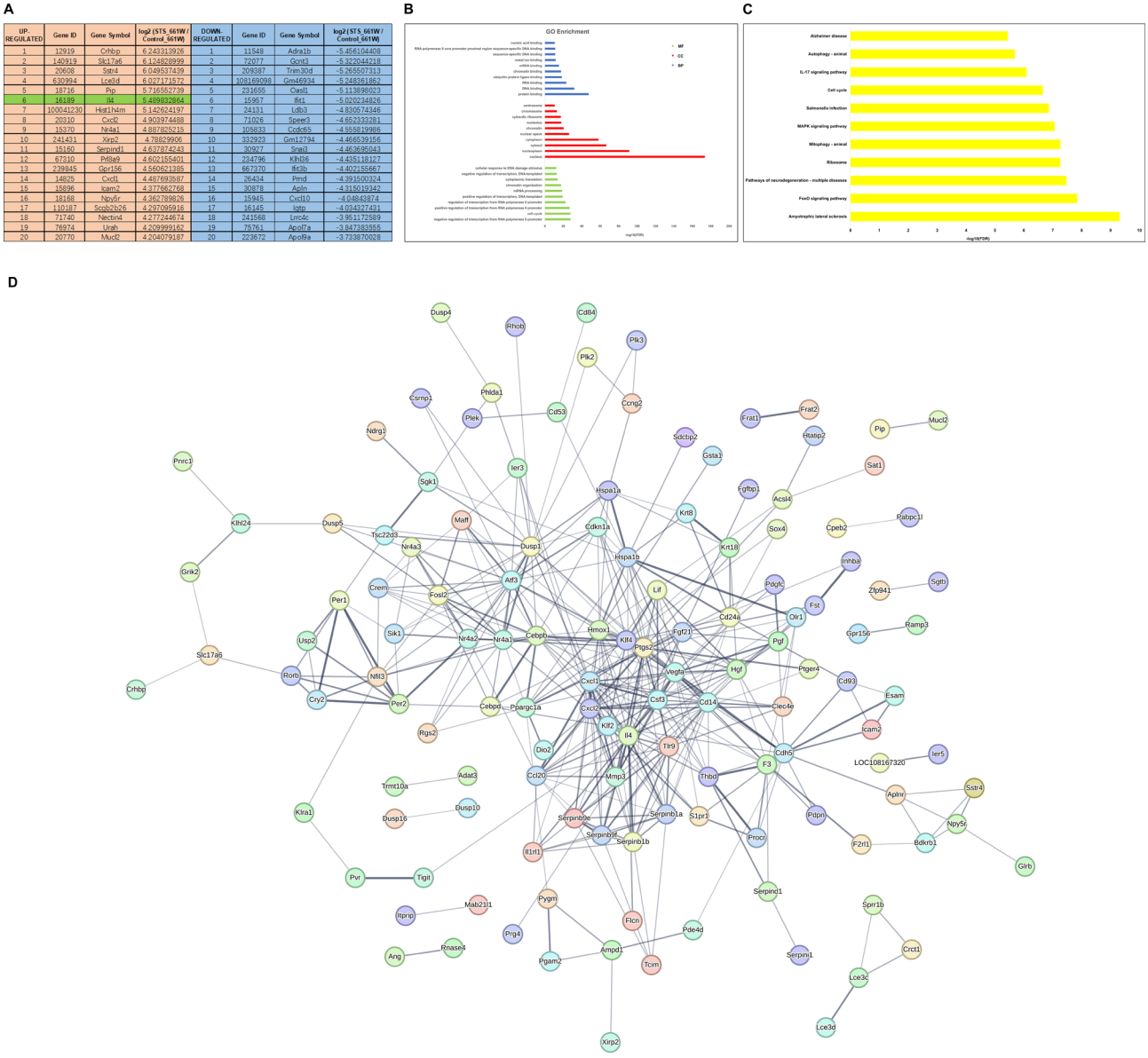

Fig. 2 Enrichment analysis of upregulated mRNAs in STS-treated 661 W cells. **A**: Differentially expressed mRNAs in 661 W cells treated with STS compared with 661 W cells treated with vehicle were ranked according to the changes in transcriptional levels. The top twenty upregulated or downregulated mRNAs are listed. IL-4 was located at the 6th position of all upregulated mRNAs. **B**: Enrichment analysis of biological process, cellular component and molecular function of upregulated mRNAs. **C**: KEGG pathway enrichment analysis results. **D**: Protein–protein interaction analysis of the top 200 upregulated mRNAs. IL-4 was the central node

of IL-4 receptors in mouse retinal RGCs. The biological activity of exogenous IL-4 relies on its specific interaction with IL-4 receptors present on the cell surface. Immunofluorescence staining results demonstrated that interleukin-4 receptor (IL-4R) was expressed in the inner layer neurons of the mouse retina. The subsequent double immunofluorescence staining confirmed the IL-4R was in the RGC layer (Fig. 4). These findings suggested that the recombinant IL-4 protein may exert its biological effects through receptor-mediated signaling pathways in retinal ganglion cells.

Afterward, we examined the protective efficacy of intravitreal administration of recombinant IL-4 protein (20 mM) against NMDA-induced RGC death. As depicted, treatment with recombinant IL-4 protein significantly conferred protection to RGCs on days 7 and 14 post-NMDA injury (Fig. 5A, B). The rIL-4 group exhibited a substantially higher number of surviving RGCs compared to the vehicle group (vehicle group vs. rIL-4 group, day 7: 576±41 vs. 724±51, $p<0.05$; Day 14: 457±53 vs. 612±72, $p<0.05$). On day 14, the average number of surviving RGCs in the rIL-4 group was

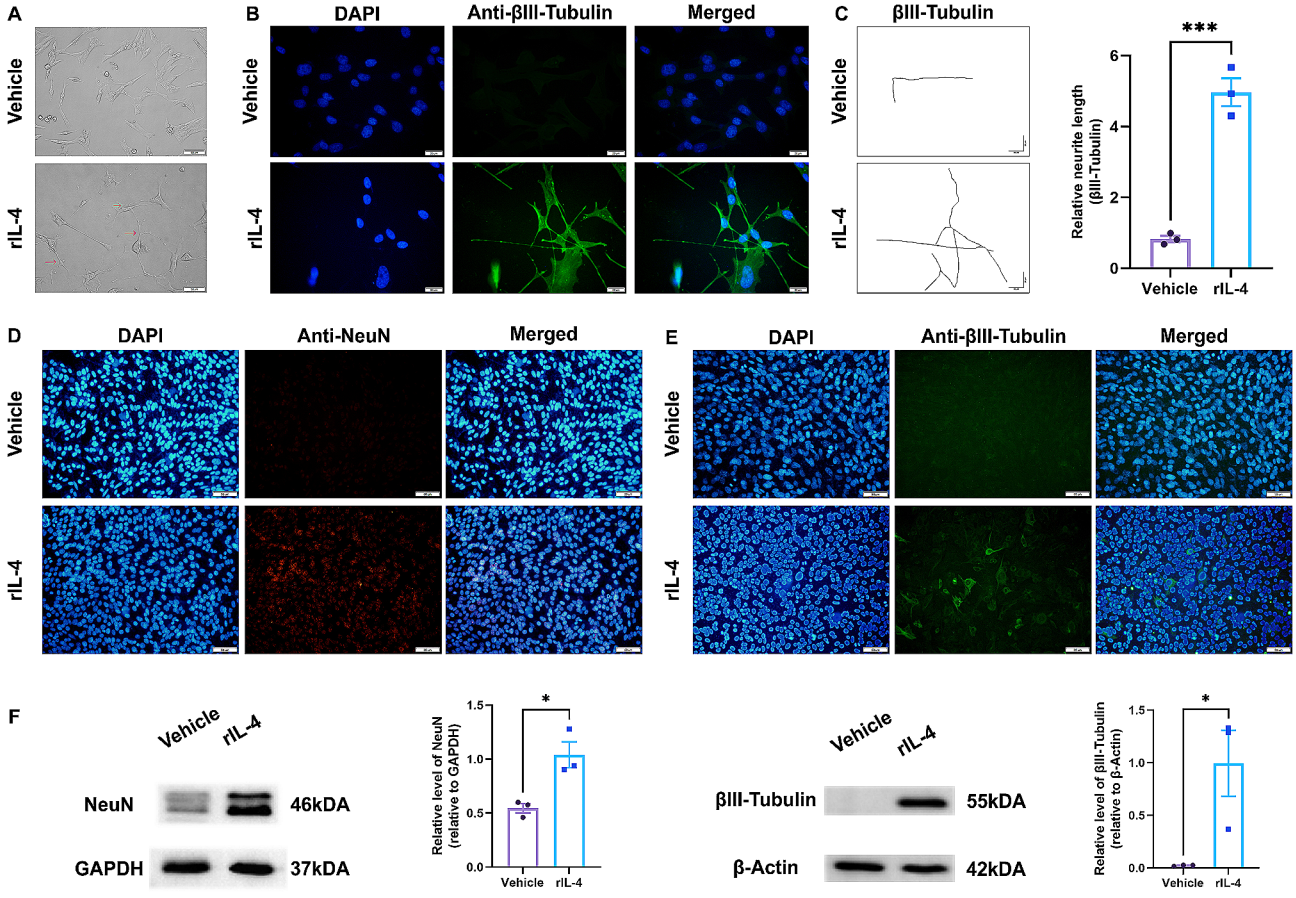

Fig. 3 Induction of axon outgrowth by recombinant IL-4 protein in 661 W cells. **A**: Light microscopy image of 661 W cells treated with vehicle and 1 μg/mL rIL-4 for 24 h. Axon-like structures (indicated by red arrows) extended from 661 W cells in the rIL-4 group. **B**: Immunofluorescence staining of βIII-tubulin showed that the axon-like structure extended from 661 W cells in the rIL-4 group was βIII-tubulin positive. **C**: Neurite tracing showed that the neurite extension length of the rIL-4 group was significantly longer than that of the vehicle group at the same treatment time. **D**, **E**, **F**: The fluorescence intensity of NeuN (red) and βIII-tubulin (green) in the rIL-4 group was higher than that in the vehicle group. Western blot results showed that the protein levels of βIII-tubulin and NeuN in the rIL-4 group were higher than those in the vehicle group. n = 3 per group, * indicates $p < 0.05$, *** indicates $p < 0.005$

approximately 1.3-fold greater than that in the vehicle group. These findings strongly indicate that recombinant IL-4 protein confers robust neuroprotection against NMDA-induced injury to RGCs.

The recombinant IL-4 protein protected RGC axons from NMDA injury

We subsequently investigated the neuroprotective effect of interleukin-4 (IL-4) on RGC axons. The structural integrity of CTB-labeled axons in the rIL-4 group was better preserved compared to the vehicle group at both 7 and 14 days post N-methyl-D-aspartate (NMDA) injury. Additionally, there was a significant increase in fluorescence intensity of CTB-labeled axons in the rIL-4 group compared to the vehicle group (Fig. 6A, B). Furthermore, immunofluorescence staining for βIII-tubulin in coronal sections of the optic nerve revealed a significantly higher number of βIII-tubulin-labeled RGC axons in the rIL-4 group on day 7 following NMDA injury (Fig. 6E, F). Moreover, we assessed long-range axon projections from RGCs and observed that on day 7 after NMDA injury, there was a significantly higher fluorescence intensity of CTB labeling in both the lateral geniculate body and superior colliculus within the rIL-4 group compared to the vehicle group (Fig. 6G, H). These findings collectively demonstrate that recombinant IL-4 protein confers protection against NMDA-induced neurotoxicity and preserves long-range axon projection.

We also conducted flash electroretinogram (ERG) recordings to observe the potential of rIL-4 in improving visual function in the NMDA model. We found that vehicle group exhibited a significant decrease in pSTR amplitude, with a reduction of 69.9 μV at day 7. In contrast, the rIL-4 group experienced a smaller decrease in pSTR amplitude, with a reduction of 28.1 μV. Additionally, the vehicle group displayed a decrease in PhNR (photopic negative response) amplitude by 41.7 μV, while the rIL-4 group showed a smaller decrease of 31.6 μV (Fig. 7A-D). Since pSTR and PhNR originate from RGCs, the reduced amplitudes observed in the vehicle group suggest that the

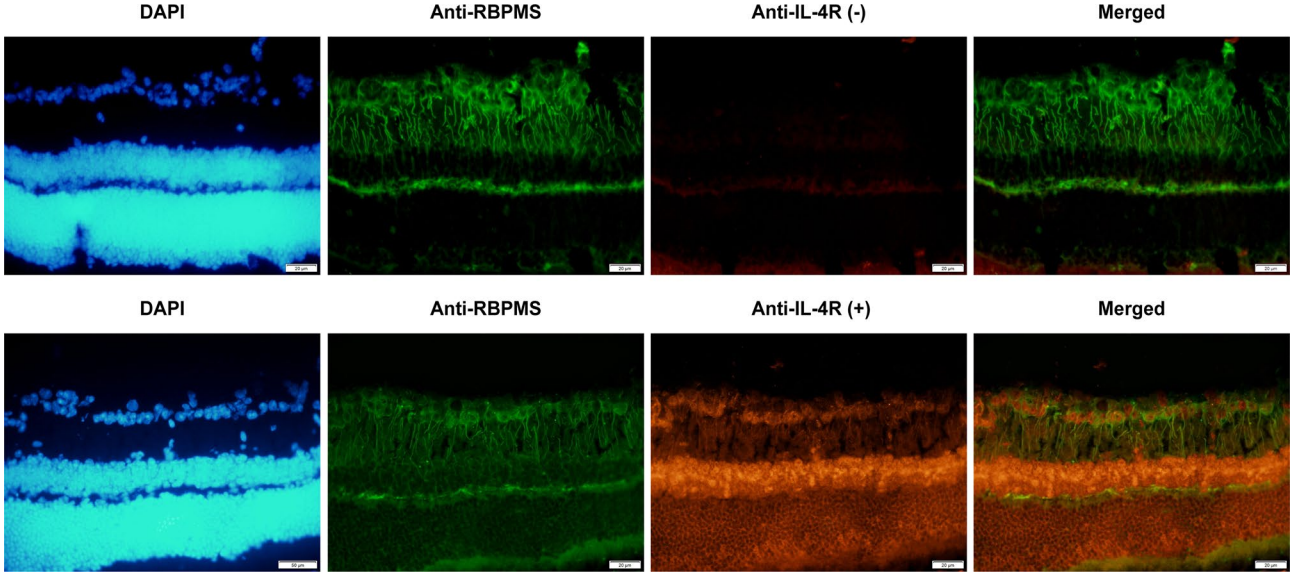

Fig. 4 IL-4 receptors expressed on mouse RGCs. RGCs were labeled with RBPMS (green), and IL-4 receptors were labeled with an IL-4R antibody (red). First row: control group without IL-4 receptor antibody incubation; Row 2: IL-4 receptor was expressed in the RGC layer. The red fluorescence labeled IL-4 receptor coincided with the green fluorescence labeled RGC, suggesting that IL-4 receptors were expressed on RGCs

function of RGCs was impaired following NMDA damage. However, rIL-4 was able to mitigate these impairments. Furthermore, rIL-4 treatment also demonstrated an improvement on the amplitude reduction of OPs, a-waves, and b-waves caused by NMDA injury (Fig. 7G, H). These findings indicate that rIL-4 holds the potential to improve visual function in the NMDA-induced retina injury.

Recombinant IL-4 protein promotes RGC axon regeneration after ONC injury

To assess the efficacy of recombinant IL-4 in the ONC model, we initially evaluated its protective effect on RGCs following ONC injury at first. On days 7 and 14 post-injury, the rIL-4 group exhibited a significantly higher number of surviving RGCs compared to the vehicle group (vehicle group vs. rIL-4 group, day 7: 682±107 vs. 888±69, $p<0.05$; day 14:585±71 vs. 759±47, $p<0.05$), indicating that IL-4 confers protection against ONC-induced RGC death (Fig. 8).

Since growth associated protein-43 (GAP43) is specifically expressed in regenerating axons, we employed CTB antegrade tracing to label RGC axons and performed GAP43 immunofluorescence staining to identify regenerated axons. The axons beyond the site of ONC injury in the rIL-4 group were found to be double-labeled by CTB and GAP43 on days 7 and 14, suggesting their regeneration as evidenced by GAP43 expression (Fig. 9A). Intravitreal administration of rIL-4 significantly enhanced RGC axon regeneration on days 7 and 14 post-injury. The number of regenerated axons extending beyond 500 μm was markedly higher in the rIL-4 group compared to the vehicle group (Fig. 9B, C). Furthermore, the longest regenerated axons reached up to 1.2 mm after ONC injury. Similarly, on days 7 and 14 post-injury, the number of GAP43-positive regenerated axons located more than 500 μm from the injury site was also significantly greater in the IL-4 group compared the vehicle group (Fig. 9D, E). These findings collectively demonstrate that recombinant IL-4 not only protects RGCs from ONC-induced injury but also promotes robust regeneration of their axonal projections.

Discussion

Staurosporine (STS), an alkaloid isolated from the culture medium of *Streptomyces staurosporesa*, is a broad-spectrum inhibitor of protein kinase C (PKC) [13]. Previous studies have demonstrated that STS induces apoptosis at micromolar concentrations. Interestingly, low concentrations of STS have been shown to significantly promote neurite outgrowth in various neuronal cell types, including HN33 hippocampal cells, RGC-5 retinal cells, PC12 pheochromocytoma cells, and SH-SY5Y neuroblastoma cells [14–16]. These findings suggest that STS may activate a common molecular mechanism underlying axon outgrowth in neurons. In this study, we investigated the key molecular targets involved in STS-mediated axon regeneration using retinal neuronal precursors (661 W cells) [17]. Consistent with previous observations, we observed a significant enhancement of axon outgrowth in 661 W cells treated with low concentrations of STS. To gain insights into the crucial molecular targets responsible for STS-induced axon regeneration, we performed whole transcriptome sequencing (mRNA-Seq) analysis

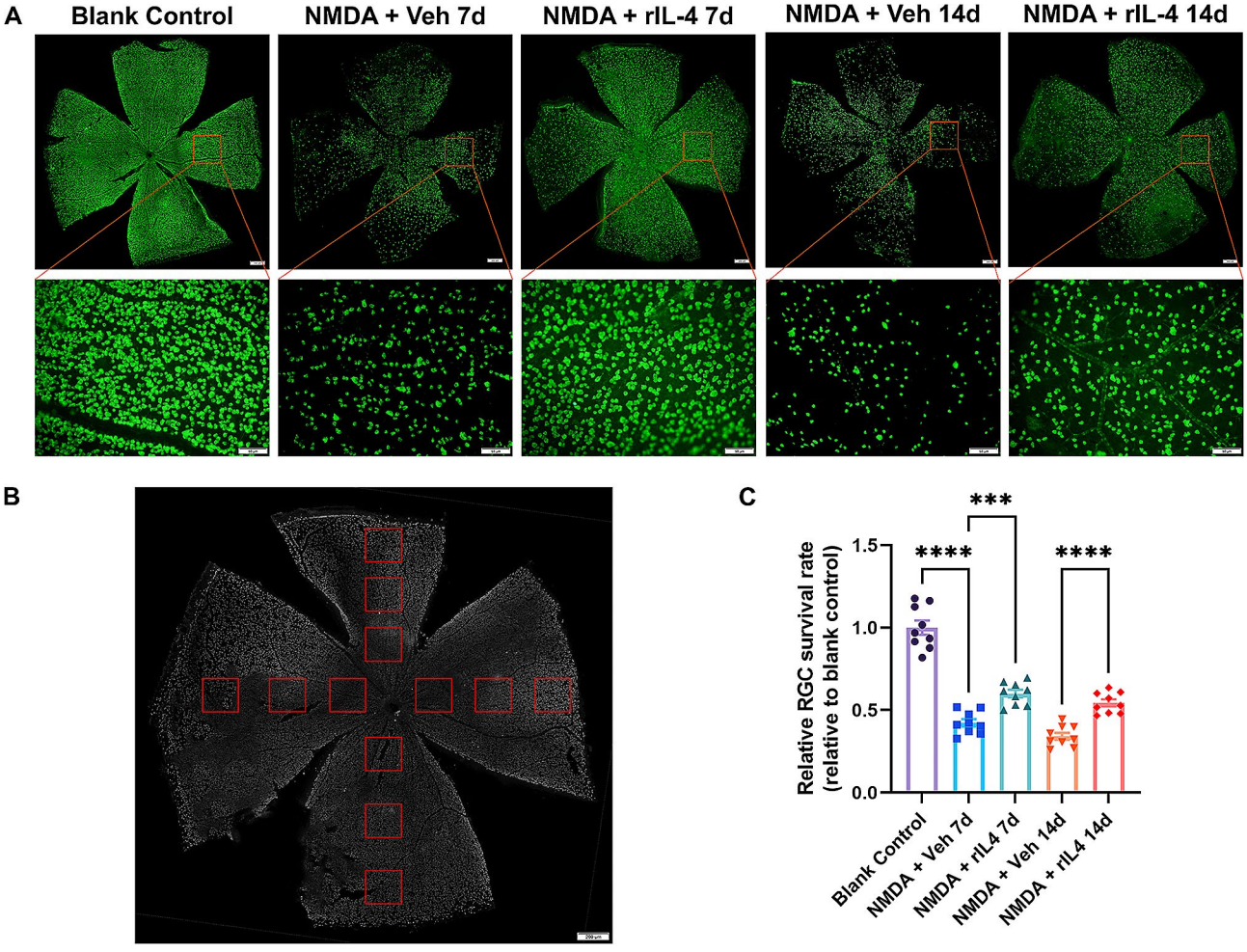

Fig. 5 Recombinant IL-4 protein reduced RGC cell death caused by NMDA injury. **A**: Immunofluorescence staining of retinal ganglion cells in the negative control group, vehicle group and rIL-4 group on day 7 and day 14 showed that the density of RGCs in the rIL-4 group was higher than that in the vehicle group at the same treatment time. **B**: Schematic diagram of the RGC counting method. A rectangle (red) indicates a high-power field of 0.38 mm×0.285 mm. The number of RGCs in each high-power field was counted, and the mean RGC number in a high-power field was calculated. The proportion of the mean RGC number of the vehicle group or rIL-4 group relative to the mean RGC number of the negative control group was calculated as the relative RGC survival rate. **C**: The relative RGC survival rate of each group. The relative RGC survival rate of the IL-4 group was greater than that of the vehicle group with the same treatment time. n = 9 eyes per group, *** indicates $p < 0.005$, **** indicates $p < 0.001$

on differentiated 661 W cells. Differential gene expression analysis revealed a significant upregulation of IL-4 gene expression upon treatment with low concentration of STS. Furthermore, protein-protein interaction analysis highlighted IL-4 as a central node regulating multiple inflammation-related signaling pathways.

Subsequently, we confirmed the ability of recombinant IL-4 protein to induce axon outgrowth in 661 W cells. Importantly, exogenous rIL-4 was also found to significantly enhance RGC axon regeneration in the mouse ONC model while providing protection against NMDA-induced retinal excitotoxic injury and preserving long-range projection of RGC axons. Previous studies have demonstrated the neuroprotective role of exogenous IL-4 in central nervous system injury. For instance, He et al. reported that administration of exogenous IL-4 at the site of injury effectively reduced neuronal apoptosis and brain tissue damage caused by cerebral ischemia in mice [18]. Pu et al. on the other hand, utilized nanoparticles for targeted delivery of IL-4 around the injured site in a mouse model of traumatic brain injury, thereby maintaining structural and functional integrity of the brain white matter and promoting transformation of oligodendrocyte precursors into myelin-generating oligodendrocytes [19]. Francos-Quijorn et al. demonstrated that exogenous IL-4 could mitigate inflammation and tissue damage following spinal cord contusions and injury, ultimately improving the spinal cord function [20]. Our findings provide initial evidence supporting an important role for IL-4 as an inflammatory factor involved in RGC axon regeneration and neuroprotection in vivo. Notably, Walsh et al. also observed a similar protective effect exerted by IL-4 on

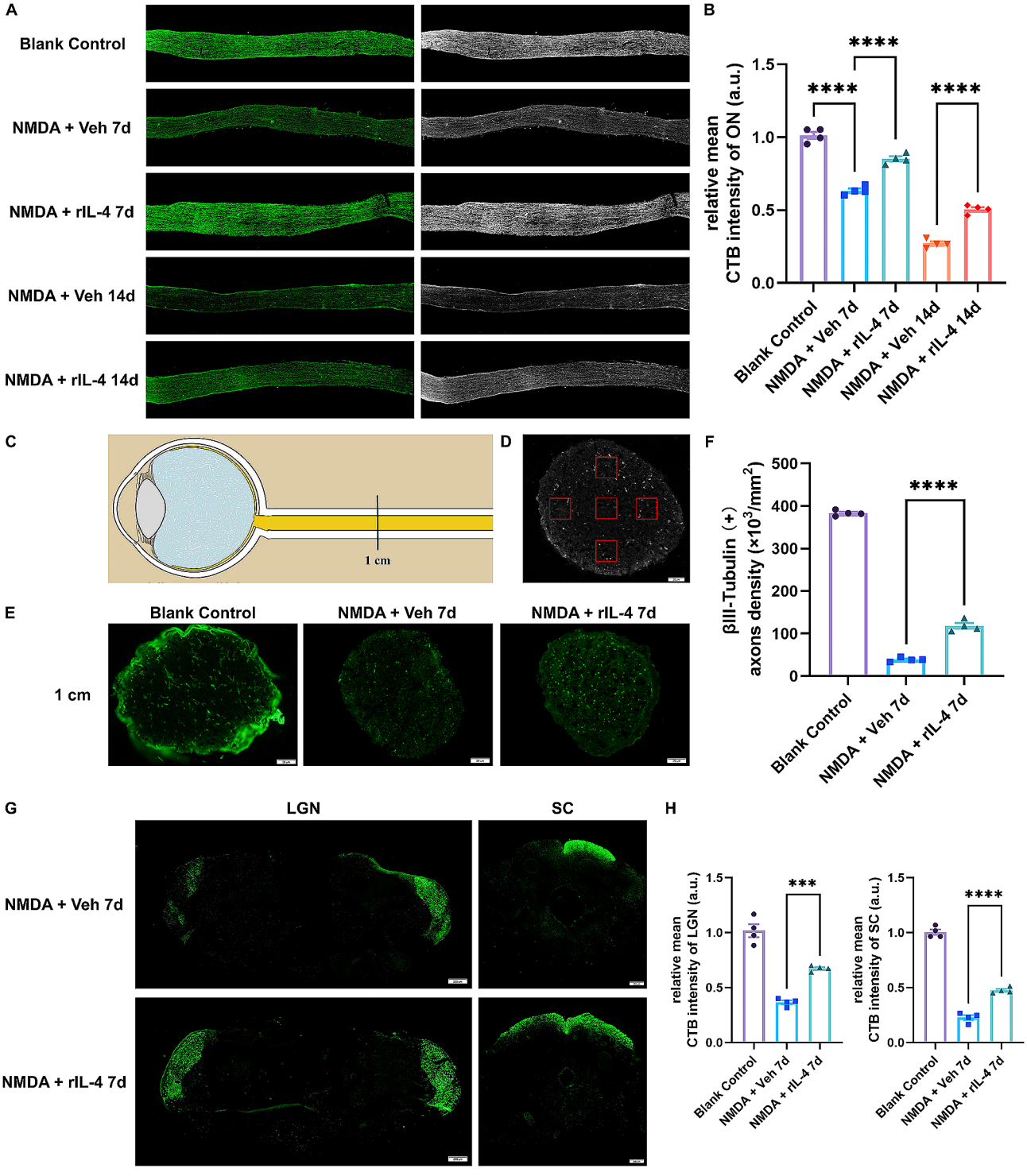

Fig. 6 Recombinant IL-4 protein attenuated NMDA-induced axon degeneration and maintained long-range axon projections in RGCs. **A**, **B**: Immunofluorescence images of retinal ganglion cell axons traced by CTB-Alexa Fluor 488. The average relative fluorescence intensity in the rIL-4 group was higher than that in the vehicle group on days 7 and 14. **C**, **D**: The cross-sectional area where axons were quantified was 1 cm distal to the injury site. The number of axons labeled with CTB was counted in five areas on a cross section of the optic nerve. Each area was 0.02×0.02 (mm^2). The mean number of CTB-labeled axons in an area was calculated. **E**, **F**: On day 7, the mean axon density labeled by CTB in the rIL-4 group was greater than that in the vehicle group. **G**, **H**: CTB labeling in the lateral geniculate body and superior colliculus of mice. On day 7, the relative fluorescence intensity of CTB in the LGN and SC in the contralateral side of rIL-4 treated eyes was significantly higher than that in the contralateral side of vehicle treated eyes. n = 4 nerves or brains, *** indicates $p < 0.005$, **** indicates $p < 0.001$

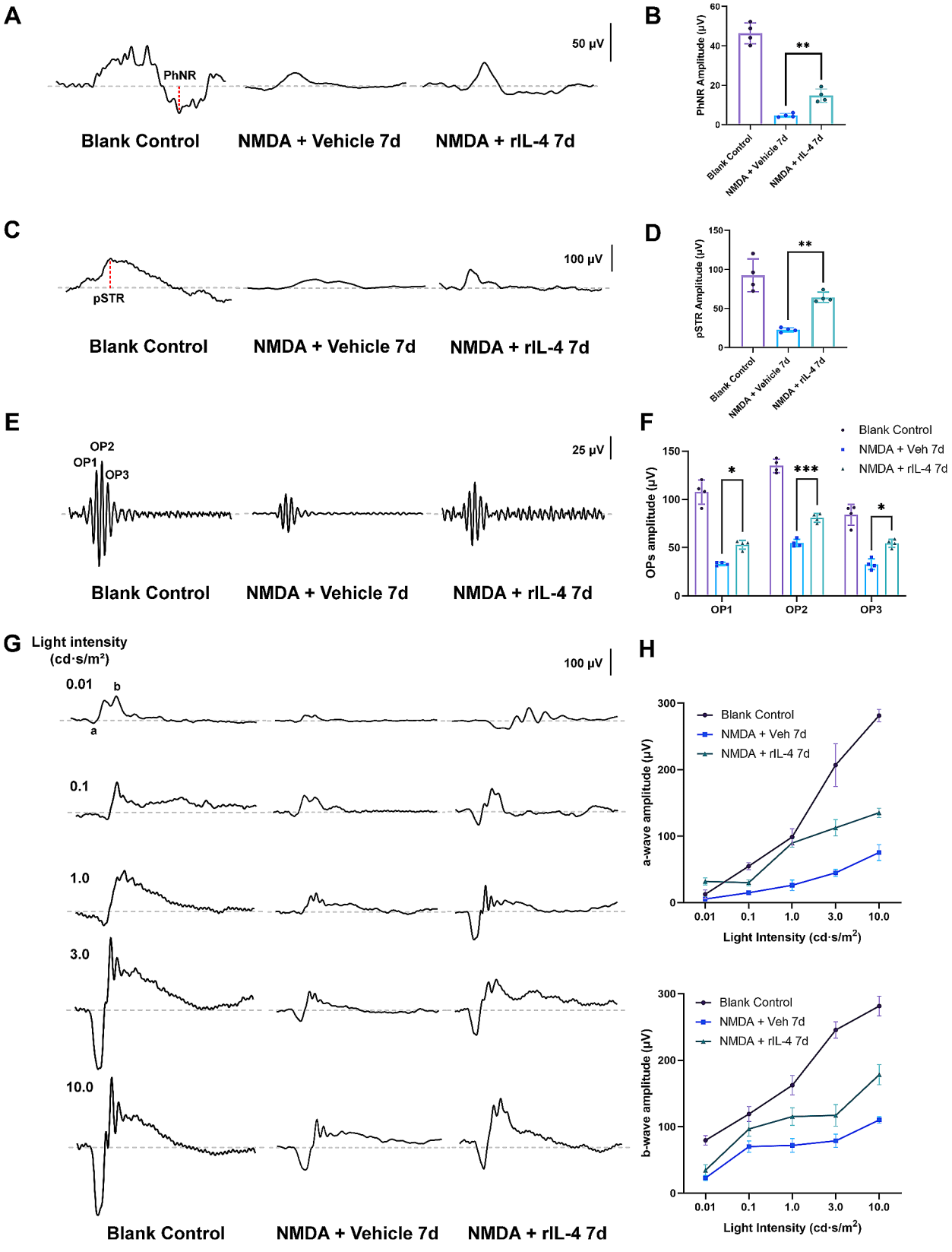

Fig. 7 (See legend on next page.)

(See figure on previous page.)

Fig. 7 rIL-4 treatment improves ERG performance in mice with NMDA-induced retina injury. **A**: Representative PhNR waveforms from eyes in blank control group, vehicle group and rIL-4 group, after 7-day NMDA damage. The PhNR was elicited with flash stimulus at an intensity of 10.0 cd·s/m^2 and measured from the baseline to the bottom of the trough following the b wave. **B**: Average amplitudes of PhNR in each group. **C**: Representative pSTR waveforms in each group. The pSTR was elicited with a flash stimulus at an intensity of 0.001 cd·s/m^2 and measured from the baseline to the following positive peak of the waveform. **D**: Average amplitudes of pSTR in each group. **E**: Representative OP waveforms in each group. The OPs were elicited with the white flashes of 3.0 cd·s/m^2 and recorded via bandpass filtering between 50 and 170 Hz. **F**: Average amplitudes of OPs (OP1, OP2, and OP3) in each group. **G**: Representative scotopic ERG responses in response to the increasing flash intensity in each group. The flash intensities used to elicit the responses are presented to the left. **H**: Average amplitudes of a- and b- waves in scotopic ERG responses, respectively. n = 4 eyes per group, * indicates $p < 0.05$, ** indicates $p < 0.01$, *** indicates $p < 0.005$

the optic nerve where they identified that $CD4^+$ T cells as mediators responsible for protecting RGCs after ONC injury [21].

Previous studies have demonstrated that both NMDA-induced injury and ONC-induced injury can ultimately result in the axon degeneration and death of RGCs [22–24]. NMDA binds to NMDA receptors, leading to an influx of calcium into cells. Calcium overload can trigger RGC death through various mechanisms, including activation of apoptotic pathways, calcium-dependent proteases activation, and generation of free radicals [25]. Following ONC injury, the axon structure is compromised, leading to axonal degeneration and retrograde RGC death due to excessive calcium influx, inflammation, oxidative stress, and other mechanisms. IL-4 has been shown to inhibit the activation of apoptosis pathway and reduce inflammation [18, 26]. Furthermore, Zhou et al. demonstrated that exogenous IL-4 could enhance the secretion of brain-derived neurotrophic factor (BDNF), ciliary neurotrophic factor (CNTF) and insulin-like growth factor-1 (IGF-1) in a mouse model of ischemic brain injury [27]. BDNF, CNTF and IGF-1 have been reported to attenuate NMDA-induced neuronal cell death [28–30]. Therefore, IL-4 may exert its protective effect on RGCs through diverse mechanisms.

On day 7 post-ONC injury, the axonal structure of RGCs distal to the injury site disintegrated in both the negative control group and the vehicle group. In contrast, regenerated RGC axons were observed in the rIL-4 group, which exhibited expression of GAP43 protein and could be traced by CTB, indicating their functional axon transport capability. Notably, our findings demonstrated that recombinant IL-4 protein exerts a prolonged effect on RGC axon regeneration lasting until at least day 14, contrary to previous studies [31]. The mechanism underlying IL-4-mediated promotion of axon regeneration is intricate. Apart from its direct action on mouse RGCs, IL-4 can induce immune cells to secrete nerve growth factors such as TGF-β2 and NGF that facilitate nerve regeneration through diverse mechanisms [32, 33]. Additionally, Golz et al. demonstrated that IL-4 promotes axon regeneration in mouse DRG cells when combined with neurotrophic factors like neurotrophin-4 (NT-4) [34]. Furthermore, inflammation-related factors contribute to neuronal cell death. For instance, Liddelow et al. reported that inflammation-induced activation of A1 astrocytes leads to cell death and axonal degeneration following ONC injury in RGCs [35]. However, a study conducted on spinal cord tissue have revealed that glial scar formation restricts short-term diffusion of inflammation at the injury site while impeding long-term axon regeneration [36]. Inflammatory factors may facilitate axon regeneration by attenuating glial scarring through promoting phagocytosis of debris, clearance of debris, and sprouting of axonal protrusions [37–40]. Furthermore, following central nervous system (CNS) injury, polarization of microglia and infiltrating macrophages towards an M2 phenotype with enhanced phagocytic capacity promotes myelin debris removal and reduces scar formation, thereby establishing a conducive microenvironment for axon regeneration [41]. Liu et al. demonstrated that IL-4 plays a pivotal role in facilitating M2 polarization of microglia/macrophages, thus contributing to long-term recovery after cerebral ischemic injury [42]. Additionally, Park et al. revealed that IL-4 and IL-10 can promote axon regeneration in sensory neurons by mitigating inflammation and modulating local immune responses following spinal cord injury in mice [43]. In summary, IL-4 may exert its pro-regenerative effects on CNS injuries through diverse mechanisms.

Additionally, IL-4 induces the phosphorylation of STAT6 and ERK. Previous studies have demonstrated that activation of the IL-4 receptor can mediate the activation of the STAT6 signaling pathway. The phosphorylated STAT6 translocates to the nucleus where it regulates transcription of IL-4-responsive genes, ultimately leading to recruitment of the MAPK signaling cascade [44]. The recruitment of MAPK signaling, including ERK, has been shown to positively contribute to axon regeneration following injury in both central and peripheral nervous systems [45–47]. Deboy et al. provided evidence that $CD4^+$ T cells exert a protective effect on motor neurons in facial nerve transection mice through dependence on the IL-4/STAT6 signaling pathway. This protective effect was significantly weakened in IL-4 knockout mice [48]. Therefore, recombinant IL-4 protein may enhance axon regeneration in retinal ganglion cells after optic nerve crush by activating both JAK1/STAT6 and ERK signaling pathways.

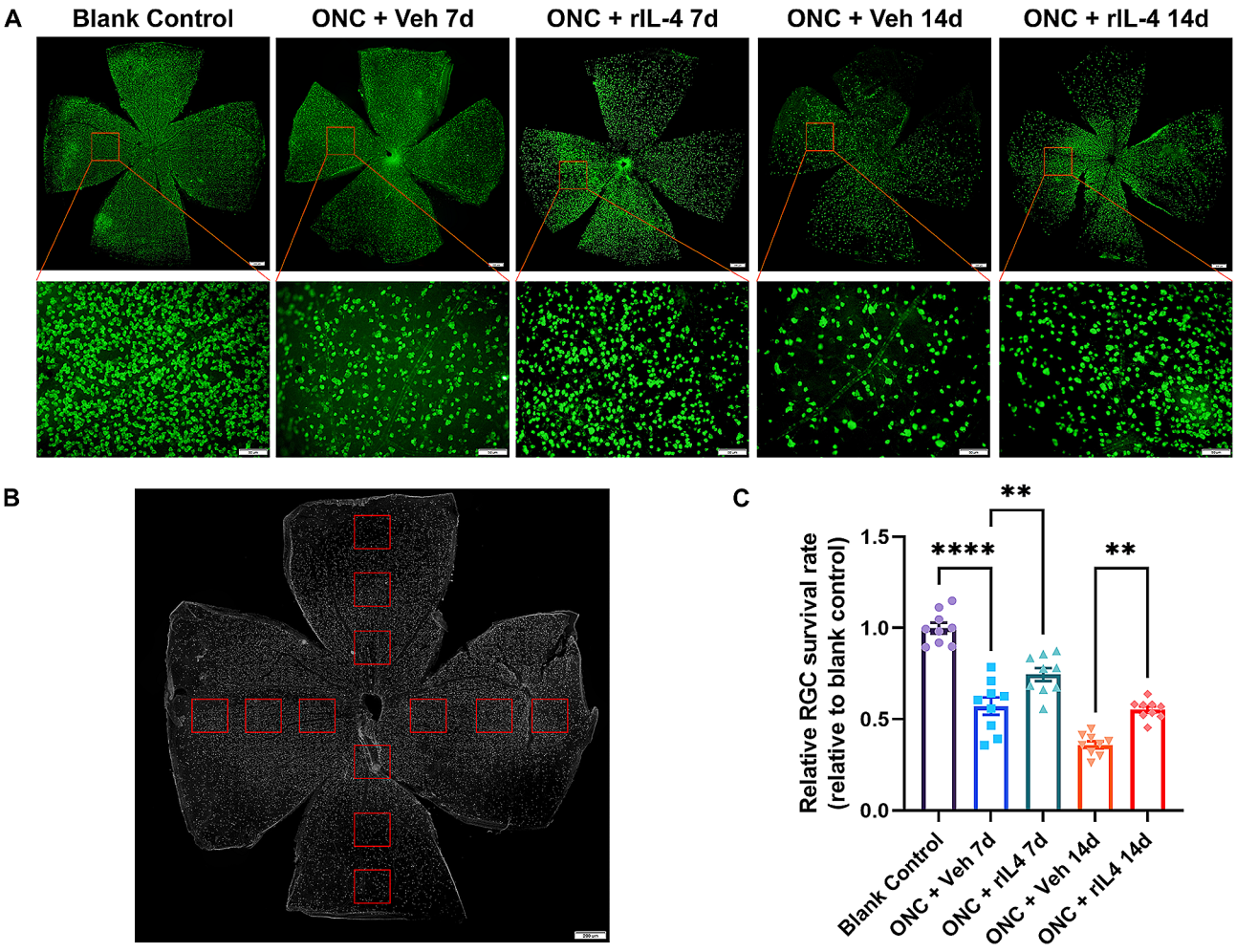

Fig. 8 Recombinant IL-4 protein reduced RGC cell death caused by ONC injury. **A**: Immunofluorescence staining of retinal ganglion cells in the negative control group, vehicle group and IL-4 group on day 7 and day 14 showed that the density of RGCs in the rIL-4 group was higher than that in the vehicle group at the same treatment time. **B**: Schematic diagram of the RGC counting method. The calculation method of the relative RGC survival rate was similar to the method of the NMDA model. **C**: Relative RGC survival rate of each group. The relative RGC survival rate of the rIL-4 group was greater than that of the vehicle group with the same treatment time. n = 9 eyes per group, ** indicates $p < 0.01$, **** indicates $p < 0.001$

Conclusion

The present study provides the initial evidence that exogenous recombinant IL-4 confers protective effects on mouse retinal ganglion cells (RGCs) against injuries induced by N-methyl-D-aspartate (NMDA) and optic nerve crush (ONC). Additionally, IL-4 preserves the integrity of long-distance RGC axon projections following NMDA injury and enhances axon regeneration in RGCs after ONC injury. Consequently, IL-4 emerges as a promising molecular target for therapeutic interventions aimed at mitigating disorders associated with RGC degeneration, such as traumatic optic neuropathy and glaucoma.

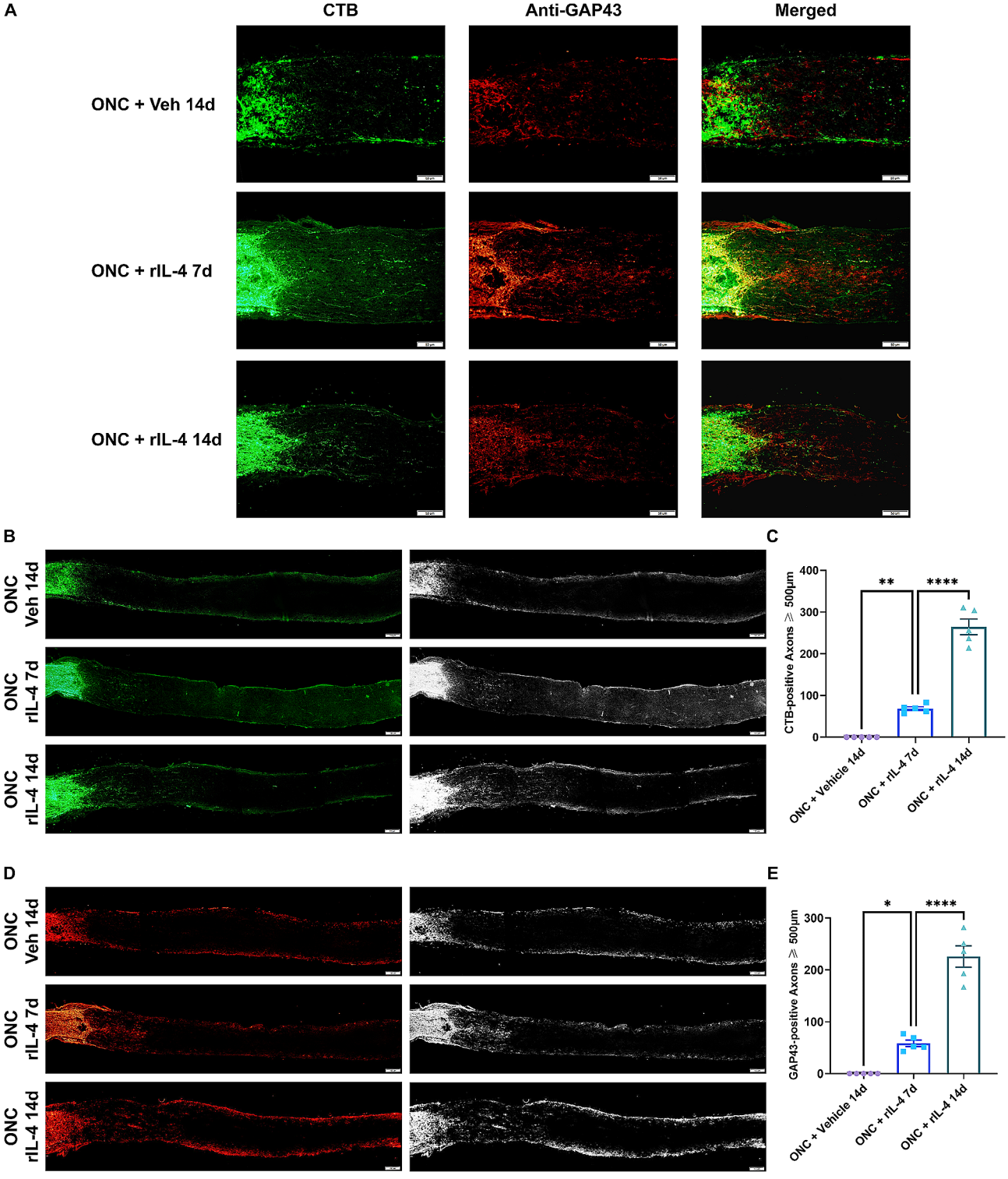

Fig. 9 RGC axon regeneration after ONC injury induced by recombinant IL-4 protein. **A**: CTB fluorescence images and GAP43 immunofluorescence staining images of axons distal to the injury site. In the rIL-4 group, there were axons labeled with both CTB (green) and GAP43 (red) distal to the injury site on days 7 and 14. The length of double-labeled axons distal to the injury site was longer in the rIL-4 treatment group on day 14 than on day 7. **B**, **C**: The number of CTB-labeled axons beyond the injury site. The number of regenerated axons with lengths greater than 500 μm beyond the injury site in the rIL-4 group was significantly higher than that on day 7 in the rIL-4 group and that on day 14 in the vehicle group. **D**, **E**: The number of axons beyond the injury site traced by GAP43 immunofluorescence staining. The number of regenerated axons with lengths greater than 500 μm beyond the injury site in the rIL-4 group was significantly higher than that on day 7 in the rIL-4 group and that on day 14 in the vehicle group. n = 5 nerves per group, * indicates $p < 0.05$, ** indicates $p < 0.01$, **** indicates $p < 0.001$

Abbreviations

AKT	protein kinase B
BDNF	brain-derived neurotrophic factor
BSA	bovine serum albumin
CCD	charge-coupled device
CNS	central nerve system
CNTF	ciliary neurotrophic factor
CTB	cholera toxin subunit B
DAPI	4′,6-diamidino-2-phenylindole
ERK	extracellular regulated protein kinases
GAP43	growth associated protein-43
IGF-1	insulin-like growth factor-1
IL-4	interleukin-4
IL-6	interleukin-6
IL-10	interleukin-10
JAK	Janus kinase
KEGG	Kyoto Encyclopedia of Genes and Genomes
MAPK	mitogen-activated protein kinase
mTOR	mammalian target of rapamycin
NGF	nerve growth factor
NMDA	N-methyl-D-aspartic acid
NMDAR	N-methyl-D-aspartic acid receptor
ONC	optic nerve crush
PBS	phosphate buffered saline
PCR	polymerase chain reaction
PI3K	phosphatidylinositol 3 kinase
PKC	protein kinase C
PTEN	phosphatidylinositol-3,4,5-trisphosphate 3-phosphatase and dual-specificity protein phosphatase
RBPMS	RNA binding protein, mRNA processing factor
RGC	retinal ganglion cell
rIL-4	recombinant IL-4 protein
STAT3	Signal Transducer and Activator of Transcription 3
STS	staurosporine
TGF-β2	transforming growth factor-β2
TNF-α	tumor necrosis factor-α

Supplementary Information

The online version contains supplementary material available at https://doi.org/10.1186/s12964-024-01604-y.

Supplementary Material 1

Acknowledgements

We would like to thank AJE (www.aje.cn) for providing linguistic assistance during the preparation of this manuscript.

Author contributions

Z.Y Z: Conceptualization, Methodology, Investigation. B. F.: Conceptualization, Investigation, Writing– review & editing, Supervision. Z.Y.Z., Y.L. and J.C.: Methodology, Investigation. G.Y.L: Conceptualization, Writing– original draft, Writing– review & editing, Funding acquisition, Resources, Supervision.

Funding

The study was funded by the National Natural Science Foundation of China (No. 82171053, 81570864).

Data availability

No datasets were generated or analysed during the current study.

Declarations

Ethical approval and consent to participate

Mice were maintained in accordance with facility guidelines on animal welfare and with protocols approved by the Animal Experimentation Ethics Committee of Jilin University.

Consent for publication

Not applicable.

Competing interests

The authors declare no competing interests.

Author details

[1]Department of Ophthalmology, The Second Norman Bethune Hospital of Jilin University, 130041 Changchun, China

Received: 2 January 2024 / Accepted: 3 April 2024
Published online: 22 April 2024

References

1. Koh JY, Wie MB, Gwag BJ, Sensi SL, Canzoniero LM, Demaro J, et al. Staurosporine-induced neuronal apoptosis. Exp Neurol. 1995;135(2):153–9.
2. Kim YH, Gum SI, Lee TY, Shin JY, Ma JY, Kim I, et al. The neuroprotective effect of staurosporine on mouse retinal ganglion cells after optic nerve injury. Int J Clin Exp Pathol. 2017;10(7):7920–8.
3. Min JY, Park MH, Park MK, Park KW, Lee NW, Kim T, et al. Staurosporin induces neurite outgrowth through ROS generation in HN33 hippocampal cell lines. J Neural Transm (Vienna). 2006;113(11):1821–6.
4. Wakita S, Izumi Y, Nakai T, Adachi K, Takada-Takatori Y, Kume T, et al. Staurosporine induces dopaminergic neurite outgrowth through AMP-activated protein kinase/mammalian target of rapamycin signaling pathway. Neuropharmacology. 2014;77:39–48.
5. Kim YH, Chang Y, Jung JC. Staurosporine induces ganglion cell differentiation in part by stimulating urokinase-type plasminogen activator expression and activation in the developing chick retina. Biochem Biophys Res Commun. 2012;423(1):67–72.
6. Xu L, Ye X, Wang Q, Xu B, Zhong J, Chen YY, et al. T-cell infiltration, contribution and regulation in the central nervous system post-traumatic injury. Cell Prolif. 2021;54(8):e13092.
7. Fischer D. Hyper-IL-6: a potent and efficacious stimulator of RGC regeneration. Eye (Lond). 2017;31(2):173–8.
8. Bethea JR, Nagashima H, Acosta MC, Briceno C, Gomez F, Marcillo AE, et al. Systemically administered interleukin-10 reduces tumor necrosis factor-alpha production and significantly improves functional recovery following traumatic spinal cord injury in rats. J Neurotrauma. 1999;16(10):851–63.
9. Lindborg JA, Tran NM, Chenette DM, DeLuca K, Foli Y, Kannan R, et al. Optic nerve regeneration screen identifies multiple genes restricting adult neural repair. Cell Rep. 2021;34(9):108777.
10. Bull ND, Chidlow G, Wood JP, Martin KR, Casson RJ. The mechanism of axonal degeneration after perikaryal excitotoxic injury to the retina. Exp Neurol. 2012;236(1):34–45.
11. Ribas VT, Koch JC, Michel U, Bahr M, Lingor P. Attenuation of Axonal Degeneration by Calcium Channel inhibitors improves retinal ganglion cell survival and regeneration after Optic nerve crush. Mol Neurobiol. 2017;54(1):72–86.
12. Yang N, Young BK, Wang P, Tian N. The susceptibility of retinal ganglion cells to Optic nerve Injury is type specific. Cells. 2020;9(3).
13. Karaman MW, Herrgard S, Treiber DK, Gallant P, Atteridge CE, Campbell BT, et al. A quantitative analysis of kinase inhibitor selectivity. Nat Biotechnol. 2008;26(1):127–32.
14. Min JY, Park MH, Park MK, Park KW, Lee NW, Kim T, et al. Staurosporin induces neurite outgrowth through ROS generation in HN33 hippocampal cell lines. J Neural Transm. 2006;113(11):1821–6.
15. Thompson AF, Levin LA. Neuronal differentiation by analogs of staurosporine. Neurochem Int. 2010;56(4):554–60.
16. Lee HG, Kim SY, Kim DS, Seo SR, Lee S-I, Shin DM, et al. 1H- 1,2,4 Oxadiazolo 4,3-a Quinoxalin-1-One inhibits Neurite Outgrowth and causes Neurite Retraction in PC12 cells independently of Soluble Guanylyl Cyclase. J Neurosci Res. 2009;87(1):269–77.
17. Sayyad Z, Sirohi K, Radha V, Swarup G. 661 W is a retinal ganglion precursor-like cell line in which glaucoma-associated optineurin mutants induce cell death selectively. Sci Rep-Uk. 2017;7.
18. He Y, Gao Y, Zhang Q, Zhou G, Cao F, Yao S. IL-4 switches Microglia/macrophage M1/M2 polarization and alleviates neurological damage by modulating the JAK1/STAT6 pathway following ICH. Neuroscience. 2020;437:161–71.
19. Pu H, Zheng X, Jiang X, Mu H, Xu F, Zhu W, et al. Interleukin-4 improves white matter integrity and functional recovery after murine traumatic brain injury via oligodendroglial PPARgamma. J Cereb Blood Flow Metab. 2021;41(3):511–29.

20. Francos-Quijorna I, Amo-Aparicio J, Martinez-Muriana A, Lopez-Vales R. IL-4 drives microglia and macrophages toward a phenotype conducive for tissue repair and functional recovery after spinal cord injury. Glia. 2016;64(12):2079–92.
21. Walsh JT, Hendrix S, Boato F, Smirnov I, Zheng J, Lukens JR, et al. MHCII-independent CD4 + T cells protect injured CNS neurons via IL-4. J Clin Invest. 2015;125(6):2547.
22. Ha Y, Ochoa LF, Solomon O, Shi S, Villarreal PP, Li S, et al. Light-sheet Microscopy of the Optic nerve reveals Axonal Degeneration and Microglial activation in NMDA-Induced Retinal Injury. EC Ophthalmol. 2021;12(11):23–31.
23. Nichol KA, Schulz MW, Bennett MR. Nitric oxide-mediated death of cultured neonatal retinal ganglion cells: neuroprotective properties of glutamate and chondroitin sulfate proteoglycan. Brain Res. 1995;697(1–2):1–16.
24. Minzenberg M, Berkelaar M, Bray G, McKerracher L. Changes in retinal ganglion cell axons after optic nerve crush: neurofilament expression is not the sole determinant of calibre. Biochem Cell Biol. 1995;73(9–10):599–604.
25. Lambuk L, Jafri AJ, Arfuzir NN, Iezhitsa I, Agarwal R, Rozali KN, et al. Neuroprotective effect of Magnesium Acetyltaurate against NMDA-Induced excitotoxicity in Rat Retina. Neurotox Res. 2017;31(1):31–45.
26. Zamorano J, Wang HY, Wang LM, Pierce JH, Keegan AD. IL-4 protects cells from apoptosis via the insulin receptor substrate pathway and a second independent signaling pathway. J Immunol. 1996;157(11):4926–34.
27. Zhou D, Ji L, Chen Y. TSPO modulates IL-4-Induced Microglia/Macrophage M2 polarization via PPAR-gamma pathway. J Mol Neurosci. 2020;70(4):542–9.
28. Wang Y, Wang W, Li D, Li M, Wang P, Wen J, et al. IGF-1 alleviates NMDA-induced excitotoxicity in cultured hippocampal neurons against autophagy via the NR2B/PI3K-AKT-mTOR pathway. J Cell Physiol. 2014;229(11):1618–29.
29. Fischer AJ, Schmidt M, Omar G, Reh TA. BMP4 and CNTF are neuroprotective and suppress damage-induced proliferation of Muller glia in the retina. Mol Cell Neurosci. 2004;27(4):531–42.
30. Martire A, Pepponi R, Domenici MR, Ferrante A, Chiodi V, Popoli P. BDNF prevents NMDA-induced toxicity in models of Huntington's disease: the effects are genotype specific and adenosine A2A receptor is involved. J Neurochem. 2013;125(2):225–35.
31. Pan D, Schellhardt L, Acevedo-Cintron JA, Hunter D, Snyder-Warwick AK, Mackinnon SE, et al. IL-4 expressing cells are recruited to nerve after injury and promote regeneration. Exp Neurol. 2022;347:113909.
32. Zhou X, Spittau B, Krieglstein K. TGFbeta signalling plays an important role in IL4-induced alternative activation of microglia. J Neuroinflammation. 2012;9:210.
33. Brodie C, Goldreich N, Haiman T, Kazimirsky G. Functional IL-4 receptors on mouse astrocytes: IL-4 inhibits astrocyte activation and induces NGF secretion. J Neuroimmunol. 1998;81(1–2):20–30.
34. Golz G, Uhlmann L, Ludecke D, Markgraf N, Nitsch R, Hendrix S. The cytokine/neurotrophin axis in peripheral axon outgrowth. Eur J Neurosci. 2006;24(10):2721–30.
35. Liddelow SA, Guttenplan KA, Clarke LE, Bennett FC, Bohlen CJ, Schirmer L, et al. Neurotoxic reactive astrocytes are induced by activated microglia. Nature. 2017;541(7638):481–7.
36. Orr MB, Gensel JC. Spinal cord Injury scarring and inflammation: therapies targeting glial and inflammatory responses. Neurotherapeutics. 2018;15(3):541–53.
37. Yin Y, Cui Q, Gilbert HY, Yang Y, Yang Z, Berlinicke C, et al. Oncomodulin links inflammation to optic nerve regeneration. Proc Natl Acad Sci U S A. 2009;106(46):19587–92.
38. Stark DT, Anderson DMG, Kwong JMK, Patterson NH, Schey KL, Caprioli RM, et al. Optic nerve regeneration after crush Remodels the Injury Site: Molecular insights from Imaging Mass Spectrometry. Invest Ophthalmol Vis Sci. 2018;59(1):212–22.
39. Kurimoto T, Yin Y, Habboub G, Gilbert HY, Li Y, Nakao S, et al. Neutrophils express oncomodulin and promote optic nerve regeneration. J Neurosci. 2013;33(37):14816–24.
40. Baldwin KT, Carbajal KS, Segal BM, Giger RJ. Neuroinflammation triggered by beta-glucan/dectin-1 signaling enables CNS axon regeneration. Proc Natl Acad Sci U S A. 2015;112(8):2581–6.
41. Raposo C, Schwartz M. Glial scar and immune cell involvement in tissue remodeling and repair following acute CNS injuries. Glia. 2014;62(11):1895–904.
42. Liu X, Liu J, Zhao S, Zhang H, Cai W, Cai M, et al. Interleukin-4 is essential for Microglia/Macrophage M2 polarization and long-term recovery after cerebral ischemia. Stroke. 2016;47(2):498–504.
43. Park J, Decker JT, Smith DR, Cummings BJ, Anderson AJ, Shea LD. Reducing inflammation through delivery of lentivirus encoding for anti-inflammatory cytokines attenuates neuropathic pain after spinal cord injury. J Control Release. 2018;290:88–101.
44. Nelms K, Keegan AD, Zamorano J, Ryan JJ, Paul WE. The IL-4 receptor: signaling mechanisms and biologic functions. Annu Rev Immunol. 1999;17:701–38.
45. Wang Q, Fan H, Li F, Skeeters SS, Krishnamurthy VV, Song Y et al. Optical control of ERK and AKT signaling promotes axon regeneration and functional recovery of PNS and CNS in Drosophila. Elife. 2020;9.
46. Hollis ER 2nd, Jamshidi P, Low K, Blesch A, Tuszynski MH. Induction of corticospinal regeneration by lentiviral trkb-induced Erk activation. Proc Natl Acad Sci U S A. 2009;106(17):7215–20.
47. Jin LQ, Zhou Y, Li YS, Zhang G, Hu J, Selzer ME. Transcriptomes of Injured Lamprey Axon Tips: Single-Cell RNA-Seq Suggests Differential Involvement of MAPK Signaling Pathways in Axon Retraction and Regeneration after Spinal Cord Injury. Cells. 2022;11(15).
48. Deboy CA, Xin J, Byram SC, Serpe CJ, Sanders VM, Jones KJ. Immune-mediated neuroprotection of axotomized mouse facial motoneurons is dependent on the IL-4/STAT6 signaling pathway in CD4(+) T cells. Exp Neurol. 2006;201(1):212–24.

Publisher's Note